Ocean Systems Engineering, *Vol. 15, No. 1 (2025) 1-21*
https://doi.org/10.12989/ose.2025.15.1.001

Impact of padeye depth of suction caisson anchors and clump weights on floating offshore wind turbines

Hiroyoshi Hirai*

Applied Geotechnical Institute, Inc., 807, Oizumi, Hokuto, Yamanashi, 409-1502, Japan

(Received August 27, 2024, Revised October 20, 2024, Accepted October 28, 2024)

Abstract. Little analytical study has been conducted to elucidate the interactions among the suction caisson anchors, mooring chains, and the platforms of floating offshore wind turbines (FOWTs). In this paper, an analytical approach will be developed to clarify the effect of the padeye depth of suction caisson anchors in sands and the mooring clump weight on the response of the comprehensive system of the FOWT. First, to predict the tensile behavior of suction caisson anchors in sand, the equations relevant to the vertical and lateral yield resistances, the bearing capacity, and pullout were presented. Second, considering the characteristics of the moorings dependent on the horizontal load applied to FOWTs and the clump weight, an analytical approach was proposed regarding the relationships among the mooring chain configuration, the caisson padeye depth, the tensile load induced at the caisson padeye, the magnitude and location of the clump weight, and the horizontal load at the spar fairlead. Last, the relationships among the displacement, the tensile capacity, and pullout of the suction caisson anchor in sand subjected to the inclined tensile loads induced at the caisson padeye were revealed when the designed horizontal load is exerted on the spar fairlead.

Keywords: clump weight; floating offshore wind turbines; mooring; pullout; sand; suction caisson anchor; three-dimensional displacement method; ultimate load

1. Introduction

The mooring system connecting the fairlead of a FOWT to the padeye of a suction caisson anchor is transformed into the various configurations such as the catenary and the taut lines to keep the floating facility in place against the external loads. To mitigate the oscillations of the FOWT due to wind and waves, clump weights are often attached to the catenary mooring line. The anchor padeye is generally set to the 2/3 embedded depth of a suction caisson anchor. The mooring portion between the seabed and the padeye within the soil is referred to as the inverse catenary.

The effect of the vertical tensile and horizontal loads on the ultimate capacity of suction caisson anchors in sand and clay has been investigated by several researchers. From the experimental data provided by Bang *et al.* (2011) and Gao *et al.* (2013) and the analytical results presented by Ahmed and Hawlader (2015), Hirai (2017b, 2018b), and Andersen *et al.* (2005), it has been deduced that for the inclined tension applied to the padeyes of suction caisson anchors in sand and clay, the ultimate tensile capacity of the suction caisson anchors occurs at about 2/3 of the

*Corresponding author, Dr., E-mail: ojiken@eps4.comlink.ne.jp

http://www.techno-press.org/?journal=ose&subpage=7 ISSN: 2093-6702 (Print), 2093-677X (Online)

embedded depth.

The investigation into the seabed trenching due to the movement of the mooring chains was initiated by Bhattacharjee *et al.* (2014) who reported that obvious seabed trenches form in front of the suction caisson in clay. Following Bhattacharjee *et al.* (2014), the formulation of the seabed trenching formation has been presented by many researchers, e.g., Arslan *et al.* (2015), Colliat *et al.* (2018), O'Neill *et al.* (2018), Rui *et al.* (2023), Sassi *et al.* (2017), Sun *et al.* (2020), and Versteele *et al.* (2017). Attention of most of the previous studies has been focused on the seabed trenching formation induced by an interaction between the mooring line and the seabed. It seems to be often postulated that the ultimate tensile capacity of an anchor may be achieved when the padeye is set to about 2/3 of the embedded depth. By altering the padeye depth, there has been little analytical investigation to take measures against the seabed trenching formation around the padeye of the suction caisson anchor.

As FOWTs are complex structures, the design practice needs aero-hydro-servo-elastic dynamic approaches to carry out the integrated analysis of the FOWTs, e.g., Ferri and Marino (2022), Sykes, *et al.* (2023), Hall *et al.* (2024), and Ramzanpoor *et al.* (2024). In most of the previous works, however, the tensile capacity and pullout of suction caisson anchors embedded in seabed to be prescribed as the prime constraints to the mooring system have not been considered in these analyses. The mooring constraints have significant effect on the design of suction caisson anchors embedded in seabed where the soils are often classified into sand and clay and these properties are distinct from each other. Furthermore, the padeye depth of the suction caisson anchor influences the horizontal load capacity of FOWTs.

In this paper, an analytical approach will be developed to elucidate the effect of the padeye depth of suction caisson anchors in sands and the mooring clump weight on the behavior of the system of the FOWT when the horizontal load is exerted on the spar fairlead. First, the vertical displacement based on a three-dimensional displacement method for the inside and outside soils adjacent to the skirt of the caisson is employed to analyze the relationship between the vertical tensile load and the vertical displacement. Second, to predict the tensile behavior of suction caisson anchors in sand, the equations relevant to the vertical and lateral yield resistances, the bearing capacity, and pullout are adopted. Third, considering the characteristics of the mooring chain dependent on the horizontal load applied to the spar fairlead and the clump weight, an analytical approach is proposed regarding the relationships among the mooring chain configuration, the caisson padeye depth, the tensile load induced at the caisson padeye, the magnitude and location of the clump weight, and the horizontal load at the spar fairlead. Finally, the relationships among the displacement, the tensile capacity, and pullout of the suction caisson anchor in sand subjected to inclined tensile loads induced at the caisson padeye are revealed when the designed horizontal load is exerted on the spar fairlead.

A cylindrical suction caisson anchor in nonhomogeneous sand is illustrated in Fig. 1(a). The suction caisson anchor has the following input parameters: external diameter, D_e, internal diameter, D_i, thickness of the lid, t_L, and that of the skirt, t_S. The length from the seabed outside the skirt to the bottom of the skirt is h. The suction caisson anchor is subjected to vertical tensile, horizontal, and moment loads on the center of the top lid, and the vertical tensile load takes a minus sign. The seabed consists of $(n-1)$ layers of nonhomogeneous sand, and the mth layer has Young's modulus, E_{Sm}, Poisson's ratio, ν_{Sm}, and length, H_{Sm}. The mb-th sand layer is set beneath the skirt tip. The rectangular coordinates (x, y, z) system is used with the reference point (0, 0, 0) on the center of the top lid.

The discretization of the suction caisson anchor in nonhomogeneous sand is exhibited in Fig.

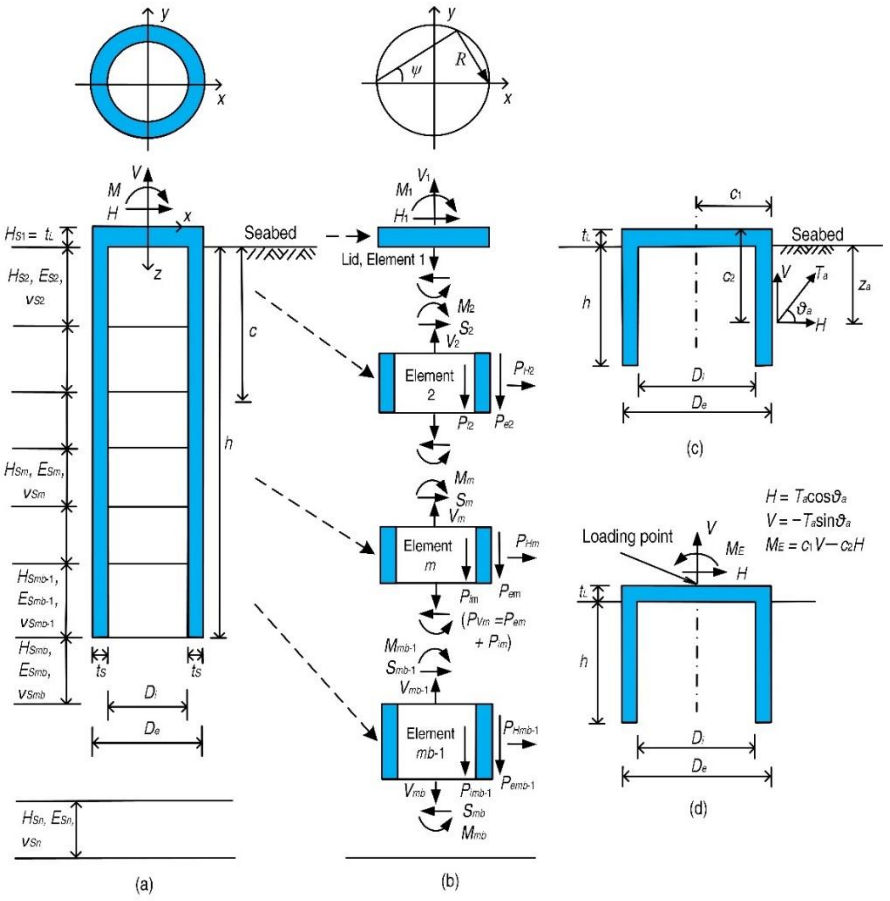

Fig. 1 (a) Suction caisson anchor, (b) discretization of nonhomogeneous sand under vertical tensile, horizontal, and moment loads, (c) inclined load at padeye, and (d) equivalent load system at top lid center

1(b) when subjected to vertical tensile, horizontal, and moment loads at the center of the top lid. V_m, M_m, and S_m represent the vertical force, moment, and shear force on the top of the mth discretized element, respectively. P_{Vm} and P_{Hm} denote the vertical and horizontal forces along the mth discretized element, respectively. The vertical force P_{Vm} comprises the internal traction, P_{im}, and the external traction, P_{em}, along the caisson wall, i.e., $P_{Vm} = P_{im} + P_{em}$. Fig. 1(c) shows that the inclined tensile load T_a at the padeye with the depth z_a from the seabed consists of the horizontal component $H = T_a \cos\theta_a$ and the vertical component $V = -T_a \sin\theta_a$, where θ_a is the inclination angle. Here c_1 is the distance between the top lid center and the outside skirt and c_2 is that between the top lid and the padeye. Fig. 1(d) shows that the system depicted in Fig. 1(c) can be transformed into an equivalent load system where the vertical (V), horizontal (H), and moment ($M_E = c_1V - c_2H$) loads are applied to the top lid center.

Hirai (2022, 2023) proposed analytical approaches based on a three-dimensional displacement method for suction caissons in sand subjected to vertical tensile, horizontal, and moment loads. The three-dimensional displacement method plays a pivotal role in analyzing the interaction

among the suction caisson anchor, the mooring, and the FOWT. Since there are a large number of equations needed in the analysis of suction caisson anchors, reiterating the main equations proposed previously will help to facilitate understanding of the present work. Therefore, the current study will describe the main equations presented formerly as well as the newly developed analytical equations relevant to catenary mooring systems with suction caisson anchors.

2. Vertical displacement of caisson

To obtain the relationship between the vertical displacement and the vertical tensile load regarding suction caisson anchors, taking into account the equilibrium of the loads exerted on the top and the skirt in the vertical direction and referring to the equation given by Hirai (2012), the vertical displacement w_1 at the reference point can be written as

$$w_1 = F_1 V_1 \tag{1}$$

where F_1 is calculated by the following recurrence equation

$$F_m = \frac{F_{m+1}+FA_m}{FB_m \cdot F_{m+1}+1} \quad (m = 1 \sim mb-1) \tag{2}$$

where the factors FA_m and FB_m are represented as follows

$$FA_m = \frac{\xi_m}{K_{Vm}} \tanh(\xi_m H_m),\ FB_m = \frac{K_{Vm}}{\xi_m} \tanh(\xi_m H_m) \tag{3}$$

The initial value F_{mb} in Eq. (2) is obtained from the relationship between displacement and base load on layered soils by assuming that the skirt base is a rigid annular punch acting on the soil surface. The factors, ξ_m and K_{Vm}, in Eq. (3) are given by

$$\xi_m = \sqrt{\frac{K_{Vm}}{A_a E_P}},\ K_{Vm} = \frac{\pi E_{em}}{I_{VV}} + \frac{\pi E_{im}}{I_{VV}} \tag{4}$$

where A_a is the area of the annular element, E_P is Young's modulus of the skirt, E_{em} and E_{im} are Young's modulus of the external sand and that of the internal sand with respect to the mth element, respectively, I_{VV} is the vertical displacement factor given by Hirai (2022, 2023), and K_{Vm} is the vertical stiffness coefficient of the mth element. The initial value F_{mb} in Eq. (2) is obtained from the relationship between vertical displacement and vertical load for the base of the skirt on multi-layered soils.

The vertical displacement, w_m, of the mth element along the skirt is given by the influence factor F_m and the vertical load V_m as follows

$$w_m = F_m V_m \tag{5}$$

where

$$V_m / V_{m-1} = 1\{FB_{m-1} \cdot F_m + cosh(\xi_{m-1} H_{sm-1})\} \tag{6}$$

The effective vertical pressure inside the skirt, σ'_{zi}, given by Janssen (1895) is written as follows

$$\sigma'_{zi} = \gamma'/\mu_i(e^{\mu_i z} - 1) \tag{7}$$

where γ' is the effective unit weight of sand and

$$\mu_i = -\frac{4K_S tan\delta}{D_i} \tag{8}$$

where K_S is the coefficient of lateral pressure, and δ is the interface friction angle between the sand and the skirt.

Houlsby *et al*. (2005) presented the effective vertical pressure outside the skirt, σ'_{ze}, as follows

$$\sigma'_{ze} = \gamma'/\mu_e(e^{\mu_e z} - 1) \tag{9}$$

where

$$\mu_e = -\frac{4K_S tan\delta}{D_e(m^2-1)} \tag{10}$$

where m is the reduction factor presented by Houlsby *et al.* (2005).

3. Lateral displacement along skirt of caisson

The lateral displacement, $u(z)$, at a depth, z, of the soil which is adjacent to a suction caisson anchor subjected to the horizontal pressure, $p_H(z)$, along the skirt can be expressed as follows:

$$u(z) = D_e I_{HH}(z)\frac{p_H(z)}{E_e(z)} \tag{11}$$

where I_{HH}, which will be presented later, is the lateral displacement factor provided by Hirai (2012).

The relationship between the lateral pressure, $p_H(z)$, and the lateral displacement, $u(z)$, in nonhomogeneous soils subjected to lateral loads is related as follows

$$p_H(z) = k_H(z)u(z) \tag{12}$$

where $k_H(z)$ is the modulus of subgrade-reaction and varies with depth z. The lateral stiffness coefficient, $K_H(z)$, along the skirt can be written as follows

$$K_H(z) = D_e k_H(z) = E_e(z)/I_{HH}(z) \tag{13}$$

When the suction caisson anchor is subjected to the lateral force, $P_H(z)$, at the depth z, the differential equation of the lateral displacement leads to the following form

$$E_P I_P \frac{d^4u(z)}{dz^4} + K_H(z)u(z) = 0 \tag{14}$$

where, I_P, is the moment of inertia of the suction caisson anchor and the lateral force, $P_H(z)$, is obtained as follows

$$P_H(z) = -K_H(z)u(z) \tag{15}$$

The solution of Eq. (14) leads to the following recurrence equation

$$\begin{pmatrix} u_{m+1} \\ \theta_{m+1} \\ M_{m+1} \\ S_{m+1} \end{pmatrix} = \begin{bmatrix} F_{1m} & -\frac{F_{2m}}{\beta_m} & -\frac{F_{3m}}{E_B I_B {\beta_m}^2} & -\frac{F_{4m}}{E_B I_B {\beta_m}^3} \\ 4\beta_m F_{4m} & F_{1m} & \frac{F_{2m}}{E_B I_B \beta_m} & \frac{F_{3m}}{E_B I_B {\beta_m}^2} \\ 4E_B I_B {\beta_m}^2 F_{3m} & -4E_B I_B \beta_m F_{4m} & F_{1m} & \frac{F_{2m}}{\beta_m} \\ 4E_B I_B {\beta_m}^3 F_{2m} & -4E_B I_B {\beta_m}^2 F_{3m} & -4\beta_m F_{4m} & F_{1m} \end{bmatrix} \begin{pmatrix} u_m \\ \theta_m \\ M_m \\ S_m \end{pmatrix} \tag{16}$$

where θ_m is the rotation of the mth element and

$\beta_m = \{K_{Hm}/(4E_P I_P)\}^{\frac{1}{4}}$,

$F_{1m} = cosh(\beta_m H_{sm}) \cdot cos(\alpha_m H_{sm})$,

$F_{2m} = \{cosh(\beta_m H_{sm})\, sin(\beta_m H_{sm}) + sinh(\beta_m H_{sm})\, cos(\beta_m H_{sm})\}/2$,

$F_{3m} = sinh(\beta_m H_{sm})\, sin(\beta_m H_{sm})/2$,

$F_{4m} = \{cosh(\beta_m H_{sm})\, sin(\beta_m H_{sm}) - sinh(\beta_m H_{sm})\, cos(\beta_m H_{sm})\}/4$,

$$\theta_{mb} = -F_{Rmb} M_{mb}, \quad u_{mb} = -F_{Hmb} S_{mb} \tag{17}$$

where m=1~mb-1; u_m, θ_m and K_{Hm} are the horizontal displacement, rotation, and the horizontal stiffness coefficient for the mth element in a suction caisson anchor, respectively; and F_{Rmb} and F_{Hmb} are the rocking and lateral influence factors on the base of the skirt, respectively (Hirai, 2017a).

Hirai (2012, 2017a-2018b, 2020, 2022, 2023) proposed the three-dimensional analytical solutions regarding piles and caissons subjected to vertical, horizontal, and moment loads. The horizontal and vertical displacement increments at the depth z, Δu and Δw, respectively, can be written as follows (Hirai 2022, 2023)

$$\Delta u = \frac{\Delta P_H}{K_H} + \frac{I_{HV}}{I_{VV}} \frac{\Delta P_V}{K_V} \tag{18}$$

$$\Delta w = \frac{I_{VH}}{I_{HH}} \frac{\Delta P_H}{K_H} + \frac{\Delta P_V}{K_V} \tag{19}$$

where ΔP_H and ΔP_V are the horizontal and vertical force increments, respectively, K_H and K_V denote the horizontal and vertical stiffness coefficients, respectively, and I_{HV}, I_{VH}, and I_{HH} are the displacement factors expressed as follows

$$K_H = \frac{E_e}{I_{HH}} \tag{20}$$

$$K_V = \frac{\pi(E_e + E_i)}{I_{VV}} \tag{21}$$

$$I_{HV} = 2 \int_0^h \int_0^{\pi/2} I_{Rz} \sin\psi \, d\psi \cdot dc \tag{22}$$

$$I_{VV} = 2 \int_0^h \int_0^{\pi/2} I_{zz} d\psi \cdot dc \tag{23}$$

$$I_{VH} = 2\int_0^h \int_0^{\pi/4} I_{zx}\cos(2\psi)d\psi \cdot dc \tag{24}$$

$$I_{HH} = 2\int_0^h \int_0^{\pi/4} I_{xx}\cos(2\psi)d\psi \cdot dc \tag{25}$$

where I_{Rz}, I_{zz}, I_{zx}, and I_{xx} are Mindlin's solutions (1936) represented by

$$I_{Rz} = \frac{(1+\nu)R}{8\pi(1-\nu)}\left\{\frac{Z_1}{{D_1}^3} + \frac{(3-4\nu)Z_1}{{D_2}^3} - \frac{4(1-\nu)(1-2\nu)}{D_2(D_2+z_2)} + \frac{6chZ_2}{{D_2}^5}\right\} \tag{26}$$

$$I_{zz} = \frac{(1+\nu)}{8\pi(1-\nu)}\left\{\frac{{Z_1}^2}{{D_1}^3} + \frac{(3-4\nu)}{D_1} + \frac{(5-12\nu+8\nu^2)}{D_2} + \frac{(3-4\nu){Z_2}^2 - 2cZ_2 + 2c^2}{{D_2}^3} + \frac{6ch{Z_2}^2}{{D_2}^5}\right\} \tag{27}$$

$$I_{zx} = \frac{(1+\nu)X}{8\pi(1-\nu)}\left\{\frac{Z_1}{{D_1}^3} + \frac{(3-4\nu)Z_1}{{D_2}^3} - \frac{6chZ_2}{{D_2}^5} + \frac{4(1-\nu)(1-2\nu)}{D_2(D_2+z_2)}\right\} \tag{28}$$

$$I_{xx} = \frac{(1+\nu)}{8\pi(1-\nu)}\left[\frac{(3-4\nu)}{D_1} + \frac{1}{D_2} + \frac{X^2}{{D_1}^3} + \frac{(3-4\nu)X^2}{{D_2}^3} + \frac{2ch}{{D_2}^3}\left(1 - \frac{3X^2}{{D_2}^2}\right) + \frac{4(1-\nu)(1-2\nu)}{D_2+z_2}\left\{1 - \frac{X^2}{D_2(D_2+z_2)}\right\}\right] \tag{29}$$

where

$$Z_1 = z - c, \qquad Z_2 = z + c, \qquad R = D_e \sin\psi, \qquad X = R\sin\psi,$$
$${D_1}^2 = R^2 + {Z_1}^2, \quad {D_2}^2 = R^2 + {Z_2}^2 \tag{30}$$

where c is the depth coordinate of node where the lateral pressure is applied and ψ is an angle shown in Fig. 1(b).

4. Yield, pullout, and failure

Hirai (2023) presented that the vertical yield resistance of the soil outside the skirt, $P_{Vye}(z)$, and that of the soil inside the skirt, $P_{Vyi}(z)$, can be written as follows

$$P_{Vye}(z) = \pi K_S \tan\delta\, \sigma'_{ze} D_e \tag{31}$$

$$P_{Vyi}(z) = \pi K_S \tan\delta\, \sigma'_{zi} D_i \tag{32}$$

For the horizontal yield resistance, $P_{Hy}(z)$, of the suction caisson anchor in sand subjected to horizontal forces, taking into account the results from Broms (1964), Fleming *et al.* (1985), and Reese *et al*. (1974) leads to the following equation

$$P_{Hy}(z) = \omega K_p \sigma'_{ze} D_e \tag{33}$$

where ω is an empirical factor, K_p is the coefficient of the Rankine passive pressure defined as $(1+\sin\varphi)/(1-\sin\varphi)$, and φ is the angle of the internal friction of sand.

Employing the vertical loads derived from Eqs. (5) and (7) and the analytical approach given by Houlsby and Byrne (2005) and Houlsby *et al.* (2005), the vertical tensile capacity, V_t, of the suction caisson anchor in sand obtained from the equilibrium in the vertical direction can be expressed as follows

$$V_t = \frac{\pi D_i^2}{4}\sum_{j=2}^{m_b-1}\gamma_j'\left\{\frac{e^{\mu_{ij}h_{j-1}}-e^{\mu_{ij}h_j}}{\mu_{ij}}+H_{sj}\right\}+\frac{\pi D_e^2(m^2-1)}{4}\sum_{j=2}^{m_b-1}\gamma_j'\left\{\frac{e^{\mu_{ej}h_{j-1}}-e^{\mu_{ej}h_j}}{\mu_{ej}}+H_{sj}\right\} \quad + W_c \quad (34)$$

where h_j is the depth of the jth layer's bottom, and γ'_j, μ_{ij}, and μ_{ej} are γ', μ_i, and μ_e of the jth layer, respectively and W_c is the buoyant weight of the suction caisson. The state where the vertical tensile load applied to the suction caisson anchor satisfies the vertical tensile capacity of Eq. (34) corresponds to pullout.

The ultimate resistance of the vertical stress (bearing capacity), σ_{zu}, for a circular base on sand is represented as

$$\sigma_{zu} = 0.5\gamma_i' B_e N_\gamma s_\gamma d_\gamma i_\gamma + \sigma'_{be} N_q s_q d_q i_q \quad (35)$$

where B_e is an effective diameter that can be calculated from the vertical and moment loads on the base, σ'_{be} is the effective vertical stress outside the caisson, and $N_q = K_p \exp(\pi\tan\varphi)$ is the bearing capacity factor proposed by Reissner (1924). Examining the calibration to match the simulated results with the experimental data presented so far and referring to the bearing capacity proposed by Hirai (2022, 2023), the appropriate bearing capacity equation used in this study consists of the following factors: the bearing capacity factor N_γ given by Michalowski (1997); the shape factors s_q and s_γ presented by Baars (2014) and Meyerhof (1963), respectively; the depth factors d_q and d_γ proposed by Meyerhof (1963) for short caissons of $h/B_e \leq 1$, and Hansen (1961, 1970) and Vesic (1973) for long caissons of $h/B_e > 1$; the inclination factors i_q and i_γ proposed by Hansen (1961, 1970).

The ultimate resistance of the shear force for the base on sand, S_u, is expressed as

$$S_u = tan\,\varphi \cdot V'_{mb} \quad (36)$$

where V'_{mb} comprises the buoyant weight of the caisson, the submerged weight of the internal soil plug, and the live vertical force V_{mb} on the caisson base.

5. Catenary mooring

Fig. 2 shows configurations of the mooring chain between the anchor and spar. Fig. 2(a) shows the system where the catenary mooring is subjected to a small horizontal load T_{sH} associated with a tension T_s and an inclination angle θ_s at the spar fairlead. The tensile load T_a with the inclination angle θ_a on the caisson padeye is induced by the horizontal load T_{sH}. The mooring chain comprises the inverse catenary denoted by S_1 inclined from the caisson padeye to Dip-Point (DP) on the seabed, the dragging line indicated by S_3 lying horizontally from DP to Touch-Point (TP) on the seabed, and the standard catenary given by S_2. Fig. 2(b) shows the case of a large horizontal load at the spar fairlead. The horizontal distances, H_1, H_2, and H_3, correspond to the lengths of projection on the seabed for the mooring chains, S_1, S_2, and S_3, respectively. For Fig. 2(c) where the chain is subjected to the small horizontal load at the spar fairlead, the tensions T_d and T_t are produced at DP and TP on the seabed, respectively, and the inclination angles θ_d and θ_t are equal to zero. For Fig. 2(d) where the chain is subjected to the large horizontal load, the tensions T_d and T_t are equivalent, and the inclination angles θ_d and θ_t are equal and have non-zero values.

In Fig. 2, the relationships between the tensions and the inclination angles are represented as follows

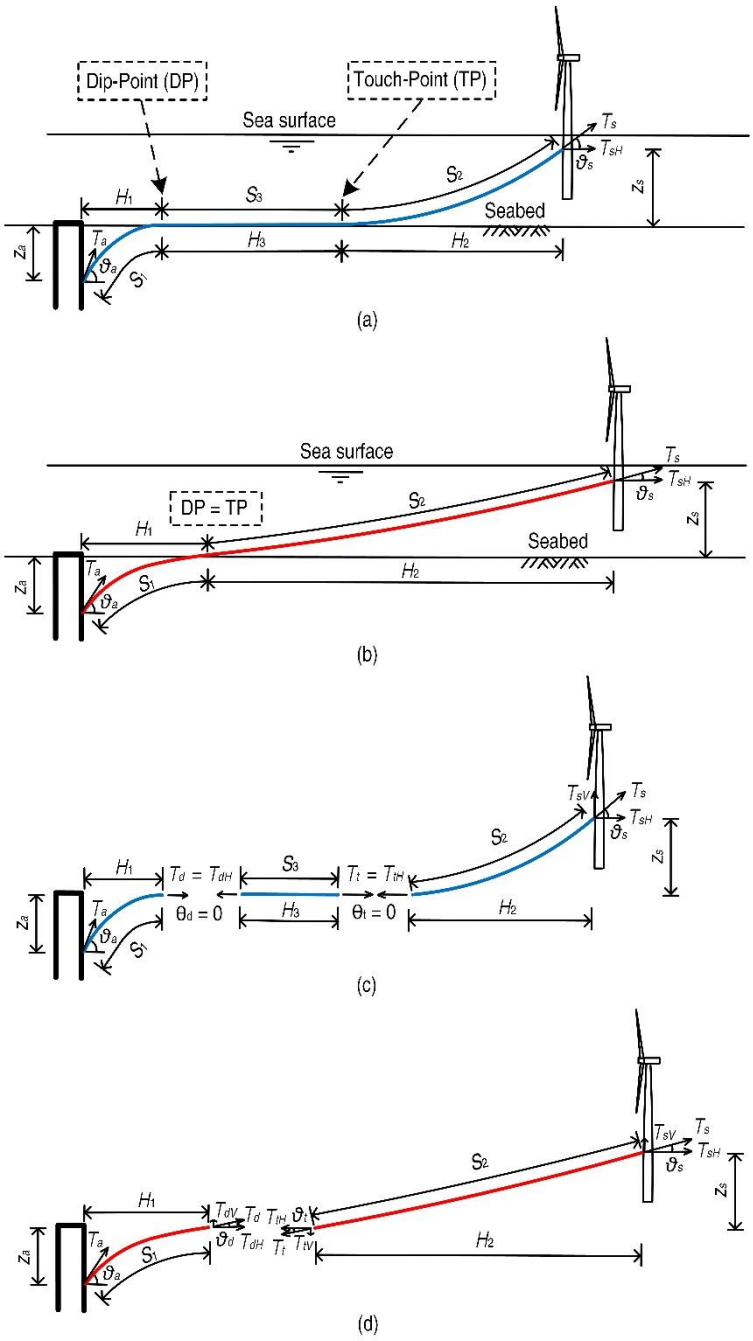

Fig. 2 Configurations of mooring chain between anchor and spar: (a) small horizontal load, (b) large horizontal load T_{sH} at spar fairlead; tensions and inclination angles relevant to mooring chain: (c) small horizontal load and (d) large horizontal load T_{sH} at spar fairlead

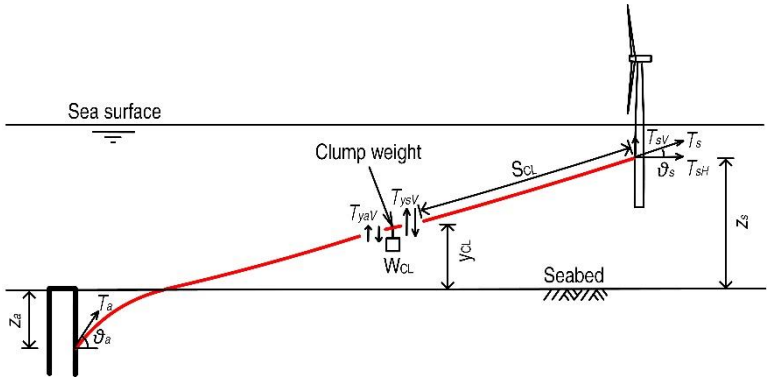

Fig. 3 Vertical components of tensions on anchor and spar sides of mooring chain using clump weight

$$T_s = T_{sH}sec\theta_s,\ T_{sV} = T_{sH}tan\theta_s,\ T_t = T_{sH}sec\theta_t,\ T_{tV} = T_{sH}tan\theta_t,\ T_{tH} = T_{sH} \tag{37}$$

The following relations hold for Fig. 2(d)

$$T_{dH} = T_{tH},\ T_{dV} = T_{tV},\ T_d = T_t,\ \theta_d = \theta_t \tag{38}$$

For the inverse catenary with the chain length of S_1, the following equations were presented by Neubecker and Randolph (1995)

$$\frac{T_a}{2}\left(\theta_a^2 - \theta_d^2\right) = z_a Q_{av},\ \ \frac{T_d}{T_a} = e^{\mu(\theta_a - \theta_d)} \tag{39}$$

where μ = frictional coefficient and Q_{av} = resistance normal to the chain per unit length given as

$$Q_{av} = \frac{1}{2}E_n d_{bar}\gamma' N_q z_a \tag{40}$$

where E_n = multiplier to give the effective width in the normal direction of the segment and d_{bar} = nominal chain diameter (i.e., diameter of the bar from which the chain is manufactured). The horizontal distance of H_1 and the chain length of S_1 are obtained as follows

$$H_1 = z_a\sqrt{2T_N}(\sqrt{1+a} - \sqrt{a}) \tag{41}$$

$$S_1 = z_a\left\{\sqrt{(1+a)(1+b)} - \sqrt{ab} + \frac{a-b}{2}\left(ln\left|\frac{\sqrt{1+a}-\sqrt{1+b}}{\sqrt{1+a}+\sqrt{1+b}}\right| - ln\left|\frac{\sqrt{a}-\sqrt{b}}{\sqrt{a}+\sqrt{b}}\right|\right)\right\} \tag{42}$$

where $T_N = T_a/(z_a Q_{av})$, $a = 0.5T_N\theta_d^2$, and $b = 0.5T_N(1+\theta_d^2)$.

The standard catenary with the chain length of S_2 is given by the following relations

$$w_{ch}S_2 = T_{sH}(tan\theta_s - tan\theta_t) \tag{43}$$

$$w_{ch}z_s = T_{sH}(sec\theta_s - sec\theta_t) \tag{44}$$

$$w_{ch}H_2 = T_{sH}\{sinh^{-1}(tan\theta_s) - sinh^{-1}(tan\theta_t)\} \tag{45}$$

where w_{ch} = buoyant weight of the chain per unit length.

For the dragging line with the chain length of S_3 on the seabed, the following relation is obtained

$$T_d = T_t - w_{ch} S_3 tan\psi \tag{46}$$

where ψ is the interface friction angle between the sand and the chain. From experimental results given by Kulhawy *et al*. (1983) and Frankenmolen *et al*. (2016), it may be assumed that $\psi = 2/3\varphi$.

Fig. 3 shows vertical components of tensions produced on the anchor and spar sides of the mooring chain using a heavy clump weight. Here, T_{yaV} and T_{ysV} represent vertical components of tensions on the anchor and spar sides of the mooring chain using the clump weight of W_{CL}, respectively, and y_{CL} and S_{CL} denote the vertical distance from the seabed and the length from the fairlead regarding the clump weight, respectively. In analysis by taking into account the clump weight, the distance of y_{CL} can be determined by using an iteration so that the solutions satisfy the catenary equations such as Eqs. (37) to (45) and the equilibrium condition of $T_{ysV} = T_{yaV} + W_{CL}$ regarding the mooring portion between the fairlead and the clump weight and that between the clump weight and the padeye.

The advantage of the analytical method developed in this work is the facilitation of the analysis for the integrated system of suction caisson anchors, moorings, and FOWTs. Eq. (42) especially has not been presented so far elsewhere in the previous works regarding the inverse catenary in sand seabed.

6. Numerical results

Little research work has been performed regarding a comprehensive analytical approach of the system of the suction caisson anchor, catenary mooring, and spar buoy. Using parameters referring to those described in the environmental statement of the Hywind Scotland Pilot Park (Statoil 2015), Arany and Bhattacharya (2018) investigated the FOWTs of spar buoy type with the catenary moorings connected to suction caisson anchors. The parameters of the FOWT, the site, and the ultimate horizontal load at the spar fairlead employed in the present paper were almost the same as those provided by Arany and Bhattacharya (2018) who presented the ultimate horizontal load which is prescribed in DNV GL (2016) as the combination of the 50-year extreme wind speed with the turbine shut down and the 50-year extreme wave height.

The parameters of the suction caisson anchor employed here were assumed as follows: external diameter D_e = 6.9 m, thicknesses of the lid and skirt are $t_L = t_S$ = 0.099 m, respectively, embedment h = 22.07 m, Young's modulus E_P = 210 GPa, and buoyant unit weight γ_c' = 68 kN/m^3. For the mooring chain, it was specified that diameter d_{bar} = 0.147 m, the length from the caisson padeye up to the spar fairlead S = 808 m, and the buoyant weight per unit length w_{ch} = 5 kN/m. The ultimate horizontal load at the spar fairlead T_{sH} = 23.1 MN and water depth z_w = 120 m were specified.

The parameters for a loose sand in seabed were assumed as follows: Young's modulus $E_s = \kappa\sigma_{at}(\sigma_m/\sigma_{at})^{\lambda}$, where a parameter κ = 400 and an exponent parameter λ = 0.6 presented by Achmus et al. (2013), σ_{at} = 100 kN/m^2 is the atmospheric pressure, $\sigma_m = (1+2K_0)\sigma'_{ze}/3$ is the mean principal stress, $K_0 = 1 - \sin\varphi$ is the in-situ coefficient of the earth pressure at rest, Poisson's ratio v_s = 0.3, internal friction angle φ = 30.0°, effective unit weight γ' = 9 kN/m^3, the parameter $K_S \tan\delta$ shown in Eqs. (11) and (12) was taken to be 0.1 according to Poulos and Davis (1980), the empirical factor $\omega = 1.43K_p$ was inferred from Fleming *et al*. (1985) and Reese *et al*. (1974), the reduction factor m =1.53 inferred from Houlsby *et al*. (2005), the multiplier E_n = 2.5 by referring to

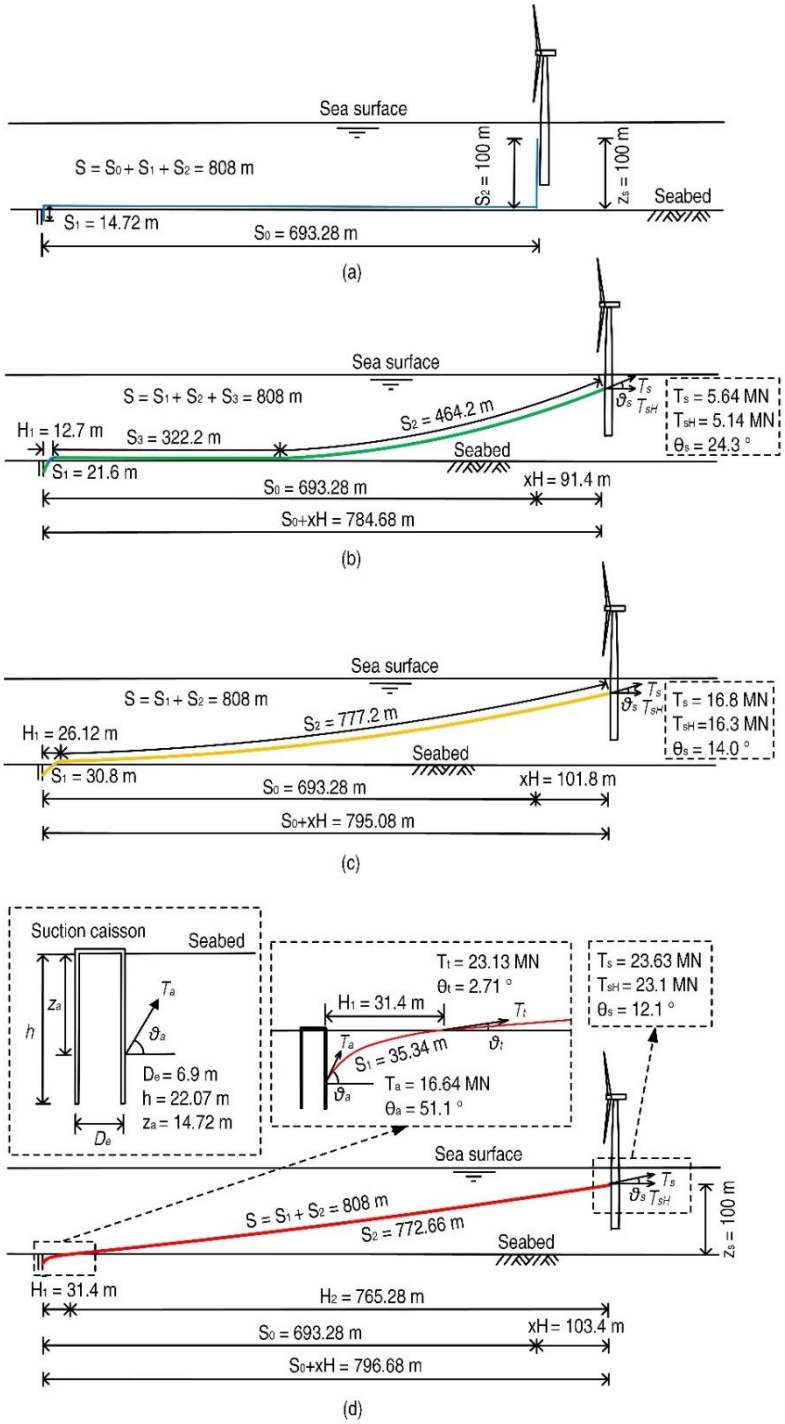

Fig. 4 Configurations of mooring chains for caissons with deep padeye depth: (a) no horizontal load, (b) T_{sH} = 5.14 MN, (c) T_{sH} =16.3 MN, and (d) T_{sH} = 23.1 MN where the horizontal load T_{sH} is applied to spar fairlead

Frankenmolen *et al*. (2016) and Neubecker and Randolph (1995), and the frictional coefficient μ = 0.39 according to Frankenmolen *et al*. (2016).

Fig. 4(a) shows the configuration of the mooring chain between the spar fairlead and the caisson with the deep padeye depth when no horizontal load is exerted on the spar fairlead. The chain length lying on the seabed is S_0 = 693.28 m, the caisson padeye depth is S_1 = 14.72 m, and the length from the spar fairlead to the seabed is $z_s = S_2$ = 100 m.

Figs. 4(b) and 4(c) show configurations of the mooring chain between the spar fairlead and the caisson padeye when the spar fairlead is subjected to the horizontal load for the caisson with the deep padeye depth. In Fig. 4(b), when the fairlead is subjected to the horizontal load of T_{sH} = 5.14 MN, the solutions are provided as follows: the tension and the inclination angle at the fairlead are T_s = 5.64 MN and θ_s = 24.3 °, respectively, the chain length from the caisson padeye to DP on the inverse catenary is S_1 = 21.6 m, the dragging line length on the seabed is S_3 = 322.2 m, the chain length from TP to the spar fairlead on the standard catenary is S_2 = 464.2 m, the projection length of S_1 on the seabed is obtained as H_1 = 12.7 m, and the horizontal displacement of the spar fairlead is calculated as xH = 91.4 m. In Fig. 4(c), when the fairlead is subjected to the horizontal load of T_{sH} = 16.3 MN, the solutions are obtained as follows: the tension and the inclination angle at the fairlead are T_s = 16.8 MN and θ_s = 14.0 °, respectively, the chain length from the caisson padeye to DP on the inverse catenary is S_1 = 30.8 m, the chain length from DP to the spar fairlead on the standard catenary is S_2 = 777.2 m, the projection length of S_1 on the seabed is given by H_1 = 26.12 m, and the horizontal displacement of the spar fairlead is calculated as xH = 101.8 m.

Fig. 4(d) shows the configuration of the mooring chain between the spar fairlead and the caisson padeye when the spar fairlead undergoes the ultimate horizontal load of T_s = 23.1 MN for the caisson with the deep padeye depth. The chain length from the caisson padeye to DP on the inverse catenary is S_1 = 35.34 m and the chain length from DP to the spar fairlead on the standard catenary is S_2 = 772.66 m. The projection lengths of S_1 and S_2 on the seabed are obtained as H_1 = 31.4 m and H_2 = 765.28 m, respectively. The horizontal displacement of the spar fairlead is calculated as xH = 103.4 m. The tension and the inclination angle at the caisson padeye are equal to T_a = 16.64 MN and θ_a = 51.1 °, respectively. The tension and the inclination angle on DP are obtained as T_t = 23.13 MN and θ_t = 2.71 °, respectively. The tension and the inclination angle on the spar fairlead are given by T_s = 23.63 MN and θ_s =12.1 °, respectively. For the caisson with the deep padeye depth, the large inclination angle at the anchor padeye arises and the large vertical component of tension tends to cause pullout of the anchor.

Fig. 5(a) shows the configuration of the mooring chain from the spar fairlead to the caisson with zero padeye depth for no horizontal load at the spar fairlead, the chain length lying on the seabed is S_0 = 708 m, and the length from the spar fairlead to the seabed is S_2 = 100 m.

Figs. 5(b) and 5(c) show configurations of the mooring chain between the spar fairlead and the caisson padeye when the spar fairlead is subjected to the horizontal load for the caisson with zero padeye depth. In Fig. 5(b), when the fairlead is subjected to the horizontal load of T_{sH} = 6.0 MN, the solutions are provided as follows: the tension and the inclination angle at the fairlead are T_s = 6.5 MN and θ_s = 22.6 °, respectively, the dragging line length on the seabed is S_3 = 308 m, the chain length from TP to the spar fairlead on the standard catenary is S_2 = 500 m, and the horizontal displacement of the spar fairlead is calculated as xH = 86.6 m. In Fig. 5(c), when the fairlead is subjected to the horizontal load of T_{sH} = 16.05 MN, the solutions are obtained as follows: the tension and the inclination angle at the fairlead are T_s = 16.55 MN and θ_s = 14.1 °, respectively, the chain length from the padeye to the spar fairlead on the standard catenary is S_2 = 808 m, and the horizontal displacement of the spar fairlead is calculated as xH = 91.7 m.

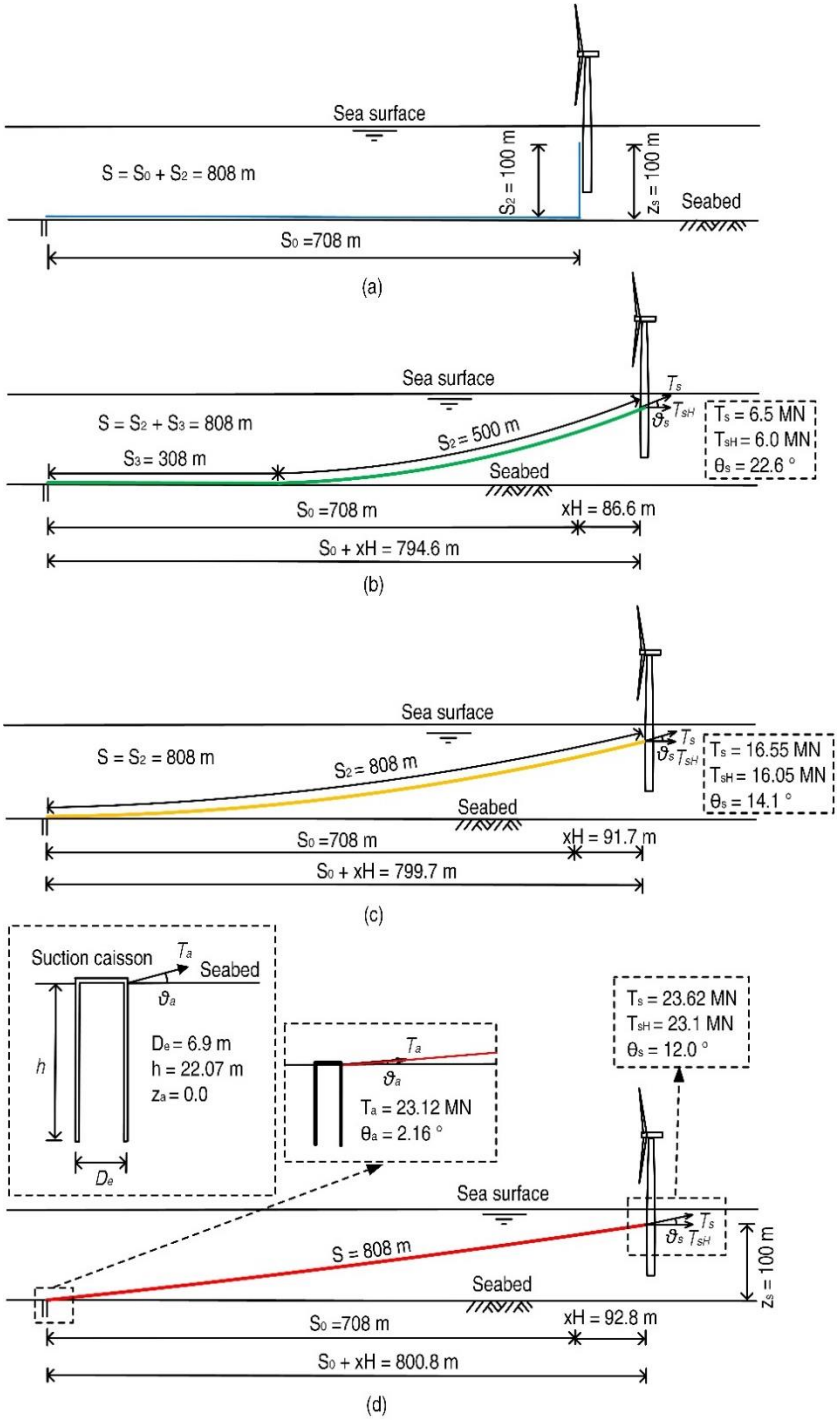

Fig. 5 Configurations of mooring chains for caissons with zero padeye depth: (a) no horizontal load, (b) T_{sH} = 6.0 MN, (c) T_{sH} = 16.05 MN, and (d) T_{sH} = 23.1 MN where the horizontal load T_{sH} is applied to spar fairlead

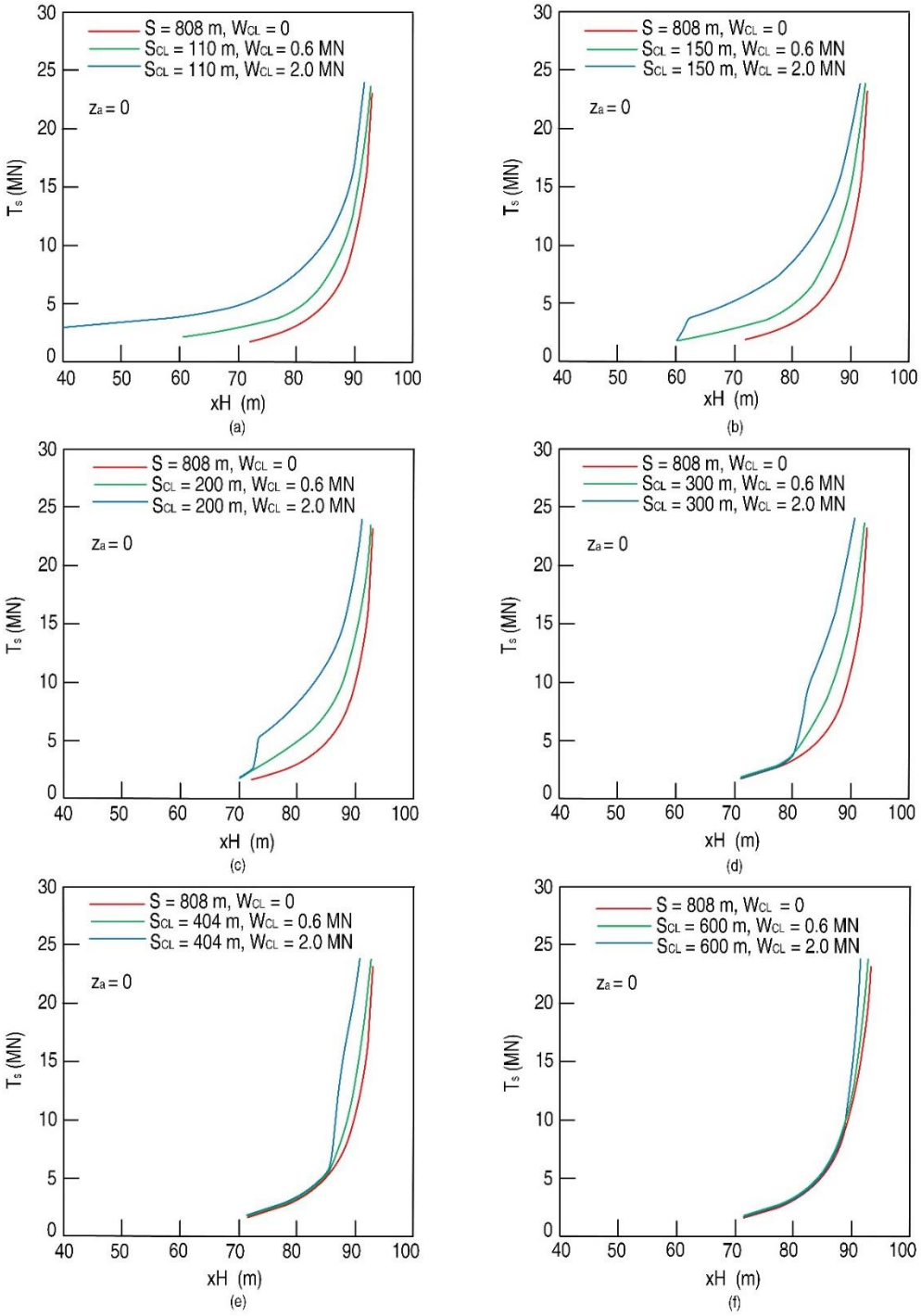

Fig. 6 Horizontal displacements at spar fairleads connected to mooring chains using clump weights for caissons with zero padeye depth: (a) S_{CL} = 110 m, (b) S_{CL} = 150 m, (c) S_{CL} = 200 m, (d) S_{CL} = 300 m, (e) S_{CL} = 404 m, and (f) S_{CL} = 600 m

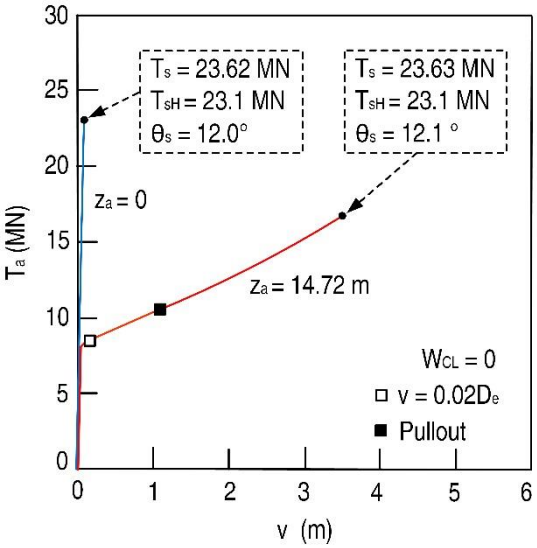

Fig. 7 Relationships between tension and displacement for caissons with zero and deep padeye depths when no clump weight

Fig. 5(d) shows the configuration of the mooring chain when the spar fairlead undergoes the ultimate horizontal load of T_{sH} = 23.1 MN for the caisson with zero padeye depth. The chain length from the caisson padeye up to the spar fairlead on the standard catenary is equal to S = 808 m. The projection length of S on the seabed is given by 800.8 m and the horizontal displacement of the spar fairlead is calculated as xH = 92.8 m. The tension and the inclination angle on the caisson padeye are equal to T_a = 23.12 MN and θ_a = 2.16 °, respectively. The tension and the inclination angle on the spar fairlead are given by T_s = 23.62 MN and θ_s = 12.0 °, respectively.

For the caisson with zero padeye depth, the small inclination angle and the insignificant vertical component of tension at the anchor padeye occur.

Figs. 6 (a) to 6(f) show the horizontal displacements at the spar fairleads connected to the mooring chains using clump weights for the caissons with zero padeye depth. Two kinds of the clump weights are taken to be W_{CL} = 0.6 and 2.0 MN, and six kinds of the mooring lengths from the fairlead to the clump weight are set as S_{CL} = 110, 150, 200, 300, 404, and 600 m. The results shown in the case of the mooring length of S =808 m and the clump weight of W_{CL}= 0 correspond to those shown in Fig. 5 where the mooring chains have no clump weights for the caissons with zero padeye depth. When the length from the fairlead to the clump weight is relatively small as shown in Figs. 6 (a) and 6(d), the effect of the clump weight on the relationship between the tension and displacement becomes more significant with increasing weight of the clump. As the mooring length from the fairlead to the clump weight increases, the influence of the clump weight on the relationship between the tension and displacement reduces. Eventually it is considered that as the length of S_{CL} of the mooring using the clump weight increases, the relationship between the tension and the displacement at the fairlead approaches that deduced from the case of S =808 m and W_{CL}= 0.

Fig. 7 shows relationships between the tension, T_a, and the displacement, v, for the caissons with zero depth and the deep padeye depth of z_a = 14.72 m, when the spar fairlead is subjected to

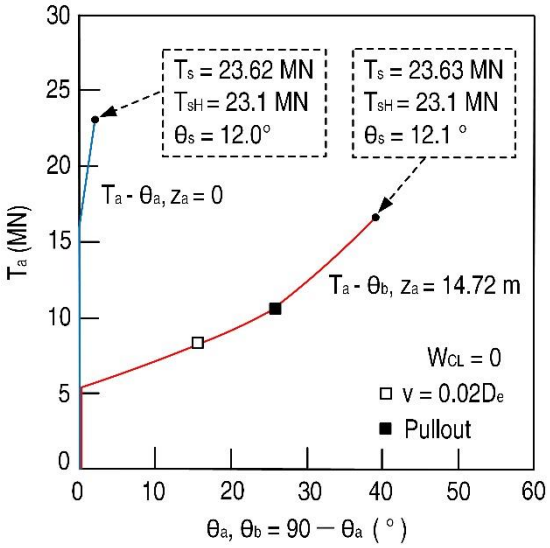

Fig. 8 Relationships between tension and inclination angle for caissons with zero and deep padeye depths when no clump weight

the horizontal load T_{sH} and the mooring has no clump weight. Here, the displacement is defined as $v = (u^2+w^2)^{1/2}$ at the reference point (0, 0, 0) in the (x, y, z) coordinates. The ultimate horizontal load is specified by T_{sH} = 23.1 MN at the spar fairlead. For the caisson with the deep padeye depth of z_a = 14.72 m, the ultimate displacement defined as $v = 0.02D_e$ = 0.138 m occurs at the tension of T_a = 8.51 MN and pullout is predicted at the displacement of v = 1.08 m and the tension of T_a = 10.6 MN. After pullout, the large displacement occurs and reaches 3.50 m at T_a = 16.64 MN and T_{sH} = 23.1 MN. For the caisson with zero padeye depth, no pullout occurs and the displacement results in 0.06 m at T_a = 23.12 MN and T_{sH} = 23.1 MN.

Fig. 8 shows relationships between the tension and the inclination angle at the caisson padeye for the caissons with zero depth and the deep padeye depth of z_a = 14.72 m, when the horizontal load T_{sH} is exerted on the spar fairlead and the mooring has no clump weight. The ultimate horizontal load is prescribed as T_{sH} = 23.1 MN at the spar fairlead. For the deep padeye depth of z_a = 14.72 m, the inclination angle θ_b = 15.7 ° arises at the tension T_a = 8.51 MN associated with the ultimate displacement of $v = 0.02D_e$ = 0.138 m. Pullout is predicted at the inclination angle θ_b = 25.8° and the tension of T_a = 10.6 MN. Following pullout, the inclination angle of θ_b becomes very large and reaches θ_b = 38.9° at T_a = 16.64 MN and T_{sH} = 23.1 MN. For the caisson with zero padeye depth, the inclination angle of θ_a = 2.16° and T_a = 23.12 MN at the padeye are generated for the ultimate horizontal load of T_{sH} = 23.1 MN at the spar fairlead. No pullout occurs and the inclination angle at the padeye eventuates in a very small value for the ultimate horizontal load at the fairlead.

Fig. 9 shows the relationships between the horizontal (H) and vertical (V) loads that compose the tension T_a at the caisson padeye for the two caisson padeye depths of z_a = 0.0 and 14.72 m when the spar fairlead undergoes the horizontal load T_{sH} and no clump weight is attached to the mooring. For the caisson with the padeye depth of z_a = 14.72 m where the ultimate horizontal load T_{sH} = 23.1 MN, the tension T_a = 16.64 MN, and the inclination angle θ_a = 51.1 ° are provided, the

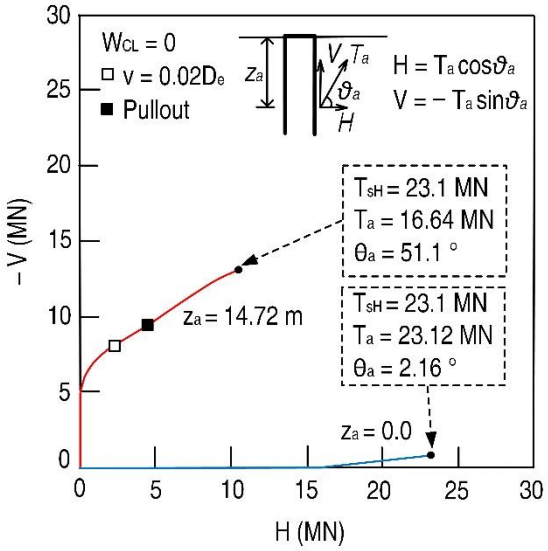

Fig. 9 Relationships between horizontal and vertical loads at caisson padeye when no clump weight

vertical and horizontal loads at the padeye are represented by V = 13.1 MN and H = 10.4 MN, respectively. For the caisson with zero padeye depth where the ultimate horizontal load T_{sH} = 23.1 MN, the tension T_a = 23.12 MN, and the inclination angle θ_a = 2.16 ° are obtained, the vertical and horizontal loads at the padeye are given as V = 0.87 MN and H = 23.0 MN, respectively. The vertical load at the padeye depth of z_a = 14.72 m is significantly greater than that at zero padeye depth.

Most of the padeyes of the suction caisson anchors in sand tend to be set at the depth of about z_a / h = 2/3, which is considered to threaten the reliability of the suction caisson anchor and the mooring system. This is because pullout tends to occur and a very large displacement follows; and furthermore, failure of the caisson anchor tends to occur due to trenching effect associated with the catenary mooring chain, as reported by Bhattacharjee *et al.* (2014).

The present study shed light on the rudimentary analytical approach of the integrated system of suction caisson anchors, moorings, and FOWTs. A comparison between the calculated results and the results obtained from experiments or actual projects has not been performed because of the dearth of appropriate measured data reflecting the integrity system. Although the issue of the reliability of the present approach will be addressed in the future, it may be considered that the minuteness of the equations adopted in the present analysis helps to enhance at least the accuracy of the numerical values in analytical results of the integrated system.

7. Conclusions

The geotechnical analyses of the mooring system connecting suction caisson anchors to FOWTs have previously not been performed sufficiently due to the complexity relevant to the mooring system. An analytical research study using a three-dimensional displacement method was carried out to predict pullout and the deformation of the suction caisson anchor through the

catenary mooring with a clump weight when the ultimate horizontal load was exerted on the spar fairlead. The conclusions are summarized as follows:

- A comprehensive analytical approach of the integrated system of suction caisson anchors, moorings, and FOWTs was proposed. The interaction among the spar buoy, the mooring chain using the clump weight, and the suction caisson anchor was clarified.
- For the relationships between the tension and deformation of the caisson anchors in sand via catenary moorings when the horizontal load was applied to the spar fairlead, it was revealed that there are significant differences of performance between the caisson with the deep padeye depth and that with zero padeye depth.
- When the mooring length from the fairlead to the clump weight is relatively small, the effect of the clump weight on the relationship between the tension and displacement at the fairlead becomes more significant with increasing weight of the clump. As the mooring length from the fairlead to the clump weight increases, the influence of the clump weight on the relationship between the tension and displacement at the fairlead reduces.
- From an examination of case studies where the ultimate horizontal load is exerted on the spar fairlead, it was found that (1) The mooring chain for the caisson anchor with the deep padeye depth comprises the standard catenary having no dragging line and the inverse catenary; (2) The mooring chain for the suction caisson anchor with zero padeye depth is composed of the standard catenary having no dragging line; and (3) The suction caisson anchor with a deep padeye depth tends to produce pullout and much larger deformation, compared to that with zero padeye depth.

References

Achmus, M., Akdag, C.T. and Thieken, K. (2013), "Load-bearing behavior of suction bucket foundations in sand", *Appl. Ocean Res*., **43**, 157-165. https://doi.org/10.1016/j.apor.2013.09.001.

Ahmed, S.S. and Hawlader, B.C. (2015), "Numerical analysis of inclined uplift capacity of suction caisson in sand", *Int. J. Offshore Polar Eng.*, **25**(2), 145-155. https://doi.org/10.17736/ijope.2015.cg11.

Andersen, K.H., Murff, J.D., Randolph, M.F., Clukey, E., Erbrich, C.T., Jostad, H.P., Hansen, B., Aubeny, C.P., Sharma, P. and Supachawarote, C. (2005), "Suction anchors for deepwater applications", *Proc. Intl. Symp. on Frontiers in Offshore Geotechnics*, (ISFOG), Perth, Australia.

Arany, L. and Bhattacharya, S. (2018), "Simplified load estimation and sizing of suction anchors for spar buoy type floating offshore wind turbines", *Ocean Eng.*, **159**, 348-357. https://doi.org/10.1061/j.oceaneng.2018.04.013.

Arslan, H., Peterman, B.R., Wang, P.C. and Bhattacharjee, S. (2015), "Remaining capacity of the suction pile due to seabed trenching", *Proceedings of the Int. Ocean and Polar Eng. Conf.*, Kona, HI, USA.

Baars, S.V. (2014), "The inclination and shape factors for the bearing capacity of footings", *Soils Found*., **54**, 985-992. https://doi.org/10.1016/j.sandf.2014.09.004.

Bang, S., Jones, K.D., Kim, K.O., Kim, Y.S. and Cho, Y. (2011), "Inclined loading capacity of suction piles in sand", *Ocean Eng.*, **38**, 915-924. https://doi.org/10.1016/j.oceaneng.2010.10.019.

Bhattacharjee, S., Majhi, S.M., Smith, D. and Garrity, R. (2014), "Serpentina FPSO mooring integrity issues and system replacement: unique fast track approach", 25449. *Proceedings of the Offshore Technology Conference*, Houston, Texas.

Broms, B.B. (1964), "Lateral resistance of piles in cohesionless soils", *J. Soil Mech. Found. Div.*, **90**, 123-156. https://doi.org/10.1061/JSFEAQ.0000614.

Colliat, J.L., Safinus, S., Boylan, N. and Schroeder, K. (2018), "Formation and development seabed trenching from subsea inspection data of deepwater Gulf of Guinea mooring", *Proceedings of the*

Offshore Techno. Conf., OCT, Houston, TX, USA.
DNV GL (2016) DNVGL-ST-0437. Loads and site conditions for wind turbines.
Ferri, G. and Marino, E. (2022), "Site-specific optimizations of a 10MW floating offshore wind turbine for the Mediterranean Sea", *Renew. Energ.*, **202**, 921-941.
Fleming, W. G. K., Weltman, A., Randolph, M. and Elson, W. (1985), Piling engineering. John Wiley and Sons, New York, USA.
Frankenmolen, S.F., White, D.J. and O'Loughlin, C.D. (2016), "Chain-soil interaction in carbonate sand". *Proc. Offshore Techno. Conf.*, OTC-27102-MS.
Gao, Y., Qiu, Y., Li, B., Li, D., Sha, C. and Zheng, X. (2013), "Experimental studies on the anti-uplift behavior of the suction caissons in sand", *Appl. Ocean Res.*, **43,** 37-45. https://doi.org/10.1016/j.apor.2013.08.001.
Hall, M., Biglu, M., Housner, S., Coughlan, K., Mahfouz, M.Y. and Lozon, E. (2024), "Floating wind farm layout optimization considering moorings and seabed variations", *J. Phys.: Confer. Series*, **2767**, 622038, IOP Publishing.
Hansen, J.B. (1961), "A general formula for bearing capacity", Geoteknisk Institute, Bulletin 11, Copenhagen.
Hansen, J.B. (1970), "A revised and extended formula for bearing capacity", Geotechnical Institute, Bulletin 28, Copenhagen.
Hirai, H. (2012), "A Winkler model approach for vertically and laterally loaded piles in nonhomogeneous soil", *Int. J. Numer. Anal. Method. Geomech.*, **36**, 1869-1897. https://doi.org/10.1002/nag.1078.
Hirai, H. (2017a), "A three-dimensional displacement approach for analysis of laterally loaded piles in nonhomogeneous soil", *Int. J. Numer. Anal. Method. Geomech.*, **41**, 1605-1635. https://doi.org/10.1002/nag.2686.
Hirai, H. (2017b), "Evaluation of pullout load capacity of suction caissons in sand using a three-dimensional displacement approach", *Mar. Georesour. Geotechnol.*, **35**(8), 1121-1134.
Hirai, H. (2018a), "Analysis of laterally loaded bucket foundation with external skirt in sand using a Winkler model approach", *Ocean Eng*., **147**, 30-44. https://doi.org/10.1016/j.oceaneng.2017.10.007.
Hirai, H. (2018b), "Analysis of pullout load capacity of suction caissons in clay by a three-dimensional displacement approach", *Mar. Georesour. Geotechnol.*, **36**(4), 425-437. https://doi/10.1080/1064119X.2017.1326070.
Hirai, H. (2020), "Analysis of cylindrical and rectangular bucket foundations subjected to vertical and lateral loads in sand using a three-dimensional displacement approach", *Soils Found*., **60**, 45-62. https://doi.org/10.1016/j.sandf.2020.01.001.
Hirai, H. (2022), "Failure surface for shallow foundations in sand using a classical bearing capacity", *Soils Found.*, **62**, 101125. https://doi.org/10.1016/j.sandf.2022.101125.
Hirai, H. (2023), "Failure envelope considering the ultimate tensile capacity of suction caissons in sand", *Soils Found.*, **63**, 101311. https://doi.org/10.1016/j.sandf.2023.101311.
Houlsby, G.T. and Byrne, B.W. (2005), "Design procedures for installation of suction caissons in sand", *Proc. Inst. Civil Eng.-Geotech. Eng.*, **158**, 135-144. https://doi.org/10.1680/geng.158.3.135.66297.
Houlsby, G.T., Kelly, R.B. and Byrne B.W. (2005), "The tensile capacity of suction caissons in sand under rapid loading", *Proceedings of the Intl. Symp. on Frontiers in Offshore Geomechanics*, ISFOG, Perth, Australia.
Janssen, H. (1895), "Versuche uber getreidedruck in silozellen", *Z. Ver. Deut. Ing.*, **39**, 1045-1049.
Kulhawy, F.H., Trautmann, C.H., Beech, J.F., O'Rourke, T.D., Mcguire, W., Wood, W.A. and Capano, C. (1983), "Transmission line structure foun.dations for uplift-compression loading", Report, Elec. Pow. Research Inst., USA.
Meyerhof, G.G. (1963), "Some recent research on the bearing capacity of foundations", *Can. Geotech. J.* **1**(1), 16-26.
Michalowski, R. (1997), "An estimate of the influence of soil weight on bearing capacity using limit analysis", *Soils Found.*, **37**, 57-64. https://doi.org/10.3208/sandf.37.4_57.
Mindlin, R.D. (1936), "Forces at a point in the interior of a semi-infinite solid.", *Physics*, **7**, 195-202.

Neubecker, S.R. and Randolph, M.F. (1995), "Profile and frictional capacity of embedded anchor chains", *J. Geotech. Eng.*, **121**(11), 797-803. https://doi.org/10.1061/(ASCE)0733-9410(1995)121:11(797).

O'Neill, M., Erbrich, C. and McNamara, A. (2018), "Prediction of seabed trench formation induced by anchor chain motions", *Proceedings of the Offshore Techno. Conf.*, OCT, Houston, TX, USA.

Poulos, H.G. and Davis, E.H. (1980), Pile foundation analysis and design. John Wiley and Sons, New York, USA.

Ramzanpoor, I., Nuernberg, M. and Tao, L. (2024), "Benchmarking study of 10 MW TLB floating offshore wind turbine", *J. Ocean Eng. Marine Ener.*, **10**, 1-34. https://doi.org/10.1007/s40722-023-00295-w.

Reese, L.C., Cox, W.R. and Koop, F.D. (1974), "Analysis of laterally loaded piles in sand", *Proceedings of the 6th Annual Offshore Tech. Conf.* 2, OTC, Houston, Texas.

Reissner, H. (1924), Zum Erddruck problem. Biezeno CB, Burgers JM (Eds), *Proceedings of the 1st Intl. Congress for Applied Mechanics*, Delft, Netherland.

Rui, S., Zhou, Z., Jostad, H.P., Wang, L. and Guo, Z. (2023), "Numerical prediction of potential 3-dimensional seabed trench profiles considering complex motions of mooring line", *Appl. Ocean Res*., **139**, 103704. https://doi.org/10.1016/j.apor.2023.103704.

Sassi, K., Kuo, M., Versteele, H., Cathie, D. and Zehzouh, S. (2017), "Insight into the mechanisms of mooring line trench formation", *Proceedings of the 8th Intl. OSIG SUT Conf.*, London.

Sun, C., Bransby, M.F., Neubecker, S.R., Randolph, M.F., Feng, X. and Gourvenec, S. (2020), "Numerical investigations into development of seabed trenching in semitaut moorings", *J. Geotech. Geoenvi. Eng.*, **146**(10), 04020098. https://doi.org/10.1061/(ASCE)GT.1943-5606.0002347.

Statoil (2015) Hywind Scotland Pilot Park – Executive Summary of the Environmental Statement.

Sykes, V., Collu, M. and Coraddu, A. (2023), "A review and analysis of optimization techniques applied to floating offshore wind platforms", *Ocean Eng*. **285**, 115247.

Vesić, A.S. (1973), "Analysis of ultimate loads of shallow foundations", *J. Soil Mech. Found. Div.*, **99**, 45-73. https://doi.org/10.1061/JSFEAQ.0001846.

Versteele, H, Kuo, M.Y.H., Cathie, D.N., Sassi, K. and Zehzouh, S. (2017), "Anchor chain trenching -Numerical simulation of progressive erosion", *Proceedings of the 8th Intl. OSIG SUT Conf*., London.

MK